

An extended polygon scaled boundary finite element method for the nonlinear dynamic analysis of saturated soil

Degao Zou^{a,b,*}, Xiaowei Teng^{a,b}, Kai Chen^{a,b}, Xiang Yu^{a,b}

^a The State Key Laboratory of Coastal and Offshore Engineering, Dalian University of Technology, Dalian, Liaoning 116024, China

^b School of Hydraulic Engineering, Dalian University of Technology, Dalian, Liaoning 116024, China

ARTICLE INFO

Keyword:

Saturated soil
Dynamic consolidation
Scaled boundary finite element method
Polygon
Pore pressure

ABSTRACT

In this paper, the polygon scaled boundary finite element method is extended to analyze saturated soil based on the generalized Biot's dynamic consolidation theory. The displacement shape functions of the polygon element are obtained by elastic static theory while the pore pressure shape functions are constructed from steady-state seepage theory. A scaled boundary polygon equations for saturated soil is established by applying Galerkin method. Two sets of Gauss points are adopted, including Gauss points of line utilized to compute the shape functions and Gauss points of area employed to realize material nonlinearity. In order to verify and assess the reliability and accuracy of the presented method, a saturated elastic half space subjected to a uniform cyclic dynamic loading is simulated and the results are compared with the analytical solution. Moreover, a liquefaction analysis of a breakwater built on saturated sand soil with generalized plastic model is subsequently carried out. The results correspond well with those calculated by finite element method (FEM), which indicates the significant capability of the current method in solving nonlinear problems. The proposed method processes extraordinary mesh flexibility and fast reconstruction, which will make it a promising tool in liquefaction analysis.

1. Introduction

As saturated soil is pervasive in the environment, its response to dynamic loading, such as earthquake, is of particular importance in a vast number of practical engineering problems. Saturated soil is a kind of saturated porous medium, which is a two-phase medium composed of a solid phase and a fluid phase. The development of pore fluid pressure during dynamic loading may significantly affect the dynamic response of a structure built on saturated soil, such as the liquefaction phenomenon in saturated sand soil. Considering the coupling interaction between solid skeletons and pore fluid, Biot [1] firstly proposed a set of governing equations which is accurate and reliable in modeling dynamic behavior of saturated porous media. Biot's theory has been applied to various problems in acoustics, geotechnical and other fields up to date. However, since the coupled partial differential equations are difficult to solve exactly, the analytical solutions are unavailable for all but the simplest problems [2–5]. Therefore, applying numerical methods, such as finite element method (FEM) and boundary element method (BEM) [6–9], is a feasible way to obtain solutions to complex problems.

The scaled boundary finite element method (SBFEM) is a semi-analytical method proposed by Song and Wolf [10–12], which combines the advantages of FEM and BEM. In this method, the discretization is only conducted in the circumferential direction and there is no need

to introduce a fundamental solution. In addition, it satisfies the singular problem automatically. Compared with conventional FEM, SBFEM provides a high precision solution with a rapid convergence rate and significantly reduces the degree of freedom in computational model [13]. These advantages make it a powerful numerical method. Since it was proposed, the method has been applied to many problems in engineering practice such as unbounded media [14], electrostatic fields [15], crack propagation [16], magneto-electro-elastic plate [17], fluid-structure interaction [18], layered soil [19] and heat conduction [20]. In unbound media problem, the boundary condition at infinity can be satisfied exactly. In crack propagation problem, the singularity can be handled without additional effort such as local mesh refinement. In fluid-structure interaction problem, since the discretization is performed only at the boundary, the number of degrees of freedom in the computational model is reduced to a large extent.

The polygon scaled boundary finite element method (PSBFEM) was recently established based on SBFEM which provides a great flexibility in modeling complex geometries and is an essential complement to the original SBFEM. Compare with FEM, it exhibits high precision with more rapid convergence rate and an advantage of solving singularity problem which is inherited from the SBFEM [21–23]. Many researchers have applied this method to their professional fields. Ooi et al. [24,25] and Dai et al. [26] applied this theory to model the crack propagation problems.

* Corresponding author at: The State Key Laboratory of Coastal and Offshore Engineering, Dalian University of Technology, Dalian, Liaoning 116024, China.
E-mail address: zoudegao@dlut.edu.cn (D. Zou).

Bao et al. [27] conducted a fracture analysis of a gravity dam under seismic loading, and Chiong et al. [28] performed a fracture analysis of functionally graded materials. Luo et al. [29] simulated a grain breakage problem using SBFEM in combination with discrete element method (DEM) where a scaled boundary polygon element is used to model an individual grain.

SBFEM is a versatile and efficient numerical method that has been widely used in various engineering and research fields as mentioned above. Nevertheless, most of the application fields are concentrated on single-phase medium and there are almost no reports about applying this method into saturated soil. In this paper, the PSBFEM is extended to the nonlinear dynamic analysis of saturated soil based on the generalized Biot's dynamic consolidation equations derived by Zienkiewicz et al. [30]. The displacement shape functions of polygon elements are constructed from the SBFEM equation of the elastic static problem while the pore pressure shape functions of polygon elements are constructed from the SBFEM equation of steady-state seepage problem. And then Galerkin method and Green formula are applied to the generalized Biot's dynamic consolidation equations, resulting in a spatially discretized scaled boundary polygon equations for dynamic analysis of saturated soil. By introducing Gauss points of area into each polygon, the material nonlinear can be considered in this equation set. The proposed method that can be discretized with arbitrary polygon and quadtree mesh is flexible in modeling complex geometry and fast and automatic in mesh generation, which makes it a competitive numerical tool in practical engineering.

The rest of this paper is organized as follows. In Section 2, the construction of scaled boundary polygon displacement shape functions and pore pressure shape functions is illustrated in details. In addition, the strain–displacement transformation matrix and the transformation matrix between pore pressure gradient and nodal pore pressures are described. The derivation of scaled boundary polygon equations for dynamic analysis of saturated soil is described in Section 3. Section 4 introduces the development platform of the proposed method. Two numerical examples are simulated to validate the reliability and accuracy of the presented method in Section 5, followed by the conclusions in Section 6.

2. Scaled boundary polygon shape functions

2.1. Coordinates transformation

An arbitrary domain can be discretized with a mesh of arbitrary n -sided polygons (where n is larger than 2). An arbitrary polygon can be treated as a SBFEM subdomain as long as the so-called scaling center O is chosen in a zone, from which the total boundary is visible. The numerical results of the domain are obtained after solving each subdomain with the SBFEM. A typical polygon modeled using the SBFEM is shown in Fig. 2.1. A scaling center is defined at the geometric center of the polygon. Each edge of the polygon is discretized using a one-dimensional line element with a local coordinate that varies from -1 to 1 , and a radial coordinate is defined that varies from 0 at the scaling center to 1 at the boundary. The Cartesian coordinates of a point on a line element with M nodes can be expressed by the scaled boundary coordinates as

$$x(\eta) = N(\eta)x_b \quad (2.1)$$

$$y(\eta) = N(\eta)y_b \quad (2.2)$$

with

$$N(\eta) = [N_1(\eta), N_2(\eta), \dots, N_M(\eta)] \quad (2.3)$$

where x_b and y_b are the vectors of nodal coordinates of a boundary line element, $x(\eta)$ and $y(\eta)$ are the coordinates along the line element, and $N(\eta)$ is the shape function vector of the line element. M can be any number larger than or equal to 2 which increases with the order of the shape functions of the line element. In this paper, first order Lagrange shape

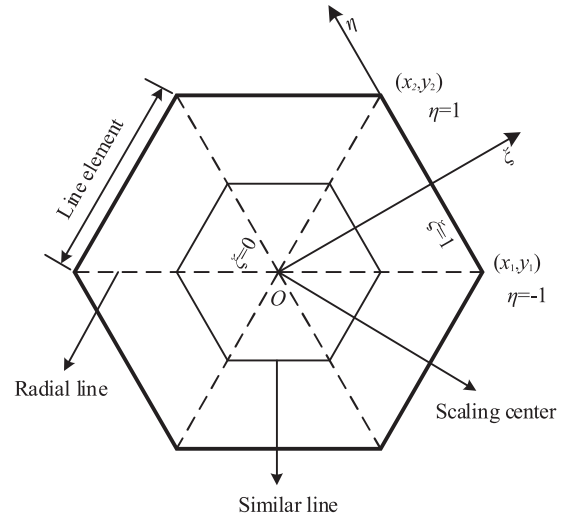


Fig. 2.1. Polygon representation for SBFEM.

functions are adopted where M equals 2. However, it is convenient to use high order shape functions without additional effort in mesh generation. The whole domain of the polygon can be described by scaling the boundaries according to the radial coordinate ξ . The Cartesian coordinates of a point within the domain with the origin at the scaling center can be given by the scaling boundary transformation equations as

$$x(\xi, \eta) = \xi N(\eta)x_b \quad (2.4)$$

$$y(\xi, \eta) = \xi N(\eta)y_b \quad (2.5)$$

2.2. The scaled boundary polygon displacement shape functions

In this study, the displacement shape functions are constructed from an elastic static equilibrium problem. Within a subdomain covered by a line element on a polygon boundary, the displacement of a point can be given as below using scaled boundary coordinates

$$u(\xi, \eta) = N_u(\eta)u(\xi) \quad (2.6)$$

where $u(\xi)$ are the radial displacement functions along a line connecting the scaling center and a node on the boundary, and $N_u(\eta)$ is the displacement shape function matrix along the circumferential direction with the following form

$$N_u(\eta) = \begin{bmatrix} N_1(\eta) & 0 & \dots & 0 & N_M(\eta) & 0 \\ 0 & N_1(\eta) & 0 & \dots & 0 & N_M(\eta) \end{bmatrix} \quad (2.7)$$

The radial displacement functions $u(\xi)$ are the solution of the SBFEM governing equations in displacement

$$E_0 \xi^2 u(\xi)_{,\xi\xi} + (E_0 - E_1 + E_1^T) \xi u(\xi)_{,\xi} - E_2 u(\xi) + F(\xi) = 0 \quad (2.8)$$

where $E_i (i=0, 1, 2)$ are coefficient matrices depending only on the geometry and material properties of the subdomain and $F(\xi)$ is a load vector including contributions from side-face traction, body force and thermal loads. When $F(\xi)=0$, the second order nonhomogeneous ordinary differential equations in Eq. (2.8) can be transformed into first order homogeneous ordinary differential equations via introducing a new vector $X(\xi)$ as below

$$X(\xi) = \begin{Bmatrix} u(\xi) \\ q(\xi) \end{Bmatrix} \quad (2.9)$$

$$\xi X(\xi)_{,\xi} = -Z X(\xi) \quad (2.10)$$

where $\mathbf{q}(\xi)$ is the internal nodal force vector and \mathbf{Z} is a Hamilton Matrix with the following form

$$\mathbf{Z} = \begin{bmatrix} \mathbf{E}_0^{-1} \mathbf{E}_1^T & -\mathbf{E}_0^{-1} \\ \mathbf{E}_1 \mathbf{E}_0^{-1} \mathbf{E}_0^T - \mathbf{E}_2 & -\mathbf{E}_1 \mathbf{E}_0^{-1} \end{bmatrix} \quad (2.11)$$

An eigenvalue decomposition of \mathbf{Z} is performed, the standard eigenvalue problem necessary for a polygon is formulated as

$$\mathbf{Z} \begin{bmatrix} \Psi_u \\ \Psi_q \end{bmatrix} = \begin{bmatrix} \Psi_u \\ \Psi_q \end{bmatrix} S_n \quad (2.12)$$

where the entries of S_n are composed of real parts of the eigenvalues which include two zeros (representing the two modes of translational rigid body motion) and native numbers, and Ψ_u and Ψ_q represent modal displacements and modal forces, respectively.

For a bounded polygon, the solution of Eq. (2.10) can be expressed as

$$\mathbf{u}(\xi) = \Psi_u \xi^{-S_n} \mathbf{c}_n \quad (2.13a)$$

$$\mathbf{q}(\xi) = \Psi_q \xi^{-S_n} \mathbf{c}_n \quad (2.13b)$$

where the coefficients \mathbf{c}_n are integration constants, which can be determined from the nodal displacement vector on the polygon boundary $\mathbf{u}_b = \mathbf{u}(\xi = 1)$

$$\mathbf{c}_n = \Psi_u^{-1} \mathbf{u}_b \quad (2.14)$$

Substituting Eq. (2.14) into Eq. (2.13a), the radial displacement functions $\mathbf{u}(\xi)$ can be expressed as

$$\mathbf{u}(\xi) = \Psi_u \xi^{-S_n} \Psi_u^{-1} \mathbf{u}_b \quad (2.15)$$

The displacement field $\mathbf{u}(\xi, \eta)$ in a sector covered by a line element on the polygon boundary can be evaluated by substituting Eq. (2.15) into Eq. (2.6) and expressed in terms of \mathbf{u}_b as

$$\mathbf{u}(\xi, \eta) = \mathbf{N}_u(\eta) \Psi_u \xi^{-S_n} \Psi_u^{-1} \mathbf{u}_b \quad (2.16)$$

The displacement shape functions of a polygon element can be extracted from the right side of Eq. (2.16) and defined as

$$\Phi_u(\xi, \eta) = \mathbf{N}_u(\eta) \Psi_u \xi^{-S_n} \Psi_u^{-1} \quad (2.17)$$

2.3. The scaled boundary polygon pore pressure shape functions

In the present method, the pore pressure shape functions are obtained from a steady-state seepage problem. The governing equation of steady-state seepage problem is a Laplace equation. Utilizing pore pressure as the variable of this equation, it can be expressed as

$$\frac{\partial}{\partial x_i} k_i \frac{\partial p}{\partial x_i} = 0 \quad (2.18)$$

The pore pressure of a point inside a sector covered by a boundary line element is defined as

$$p(\xi, \eta) = \mathbf{N}_p(\eta) \mathbf{p}(\xi) \quad (2.19)$$

with

$$\mathbf{N}_p(\eta) = [\mathbf{N}_1(\eta) \ \mathbf{N}_2(\eta) \ \cdots \ \mathbf{N}_M(\eta)] \quad (2.20)$$

where $\mathbf{p}(\xi)$ are the radial pore pressure functions along a line connecting the scaling center and a node on the boundary and $\mathbf{N}_p(\eta)$ is the pore pressure shape function vector along the circumferential direction. Applying Galerkin method and Green formula to the Laplace equation, the SBFEM governing equations is derived as

$$\mathbf{E}_0^p \xi^2 \mathbf{p}(\xi)_{,\xi\xi} + \left(\mathbf{E}_0^p - \mathbf{E}_1^p + (\mathbf{E}_1^p)^T \right) \xi \mathbf{p}(\xi)_{,\xi} - \mathbf{E}_2^p \mathbf{p}(\xi) + \mathbf{f}(\xi) = \mathbf{0} \quad (2.21)$$

where $\mathbf{E}_i^p (i = 0, 1, 2)$ are coefficient matrices which depend on the geometry parameters of the polygon and the permeability of porous media, and $\mathbf{f}(\xi)$ is a flux vector.

Eq. (2.21) is second-order nonhomogeneous ordinary differential equations. When $\mathbf{f}(\xi) = \mathbf{0}$, a new vector is introduced to solve the equations which is given as

$$\mathbf{X}_p(\xi) = \begin{Bmatrix} \mathbf{p}(\xi) \\ \mathbf{Q}(\xi) \end{Bmatrix} \quad (2.22)$$

where $\mathbf{Q}(\xi)$ is the internal nodal flux vector corresponding to $\mathbf{p}(\xi)$. This enables Eq. (2.21) to be transformed into first-order homogeneous ordinary differential equations which can be written as

$$\xi \mathbf{X}_p(\xi)_{,\xi} = -\mathbf{Z}_p \mathbf{X}_p(\xi) \quad (2.23)$$

where \mathbf{Z}_p is a Hamilton matrix with the following form

$$\mathbf{Z}_p = \begin{bmatrix} (\mathbf{E}_0^p)^{-1} (\mathbf{E}_1^p)^T & -(\mathbf{E}_0^p)^{-1} \\ \mathbf{E}_1^p (\mathbf{E}_0^p)^{-1} (\mathbf{E}_1^p)^T - \mathbf{E}_2^p & -\mathbf{E}_1^p (\mathbf{E}_0^p)^{-1} \end{bmatrix} \quad (2.24)$$

An eigenvalue decomposition of \mathbf{Z}_p is conducted, the standard eigenvalue problem necessary for a polygon is formulated as

$$\mathbf{Z}_p \begin{bmatrix} \Psi_p \\ \Psi_Q \end{bmatrix} = \begin{bmatrix} \Psi_p \\ \Psi_Q \end{bmatrix} S_n^p \quad (2.25)$$

where the entries of S_n^p are composed of real parts of the eigenvalues which include one zero (representing the one mode of translational rigid body motion) and negative numbers, and Ψ_p and Ψ_Q represent modal pore pressures and modal fluxes, respectively.

For a bounded polygon, the solution of Eq. (2.23) can be expressed as

$$\mathbf{p}(\xi) = \Psi_p \xi^{-S_n^p} \mathbf{c}_n^p \quad (2.26a)$$

$$\mathbf{Q}(\xi) = \Psi_Q \xi^{-S_n^p} \mathbf{c}_n^p \quad (2.26b)$$

where the coefficients \mathbf{c}_n^p are integration constants, which can be determined from the nodal pore pressure vector on the polygon boundary $\mathbf{p}_b = \mathbf{p}(\xi = 1)$

$$\mathbf{c}_n^p = \Psi_p^{-1} \mathbf{p}_b \quad (2.27)$$

Substituting Eq. (2.27) into Eq. (2.26a), the radial pore pressure functions $\mathbf{p}(\xi)$ can be expressed as

$$\mathbf{p}(\xi) = \Psi_p \xi^{-S_n^p} \Psi_p^{-1} \mathbf{p}_b \quad (2.28)$$

Substituting Eq. (2.28) into Eq. (2.19), the pore pressure field $\mathbf{p}(\xi, \eta)$ within a sector covered by a line element on the polygon boundary can be expressed in terms of \mathbf{p}_b as

$$p(\xi, \eta) = \mathbf{N}_p(\eta) \Psi_p \xi^{-S_n^p} \Psi_p^{-1} \mathbf{p}_b \quad (2.29)$$

The pore pressure shape functions of a polygon element can be acquired from the right side of the Eq. (2.29) and defined as

$$\Phi_p(\xi, \eta) = \mathbf{N}_p(\eta) \Psi_p \xi^{-S_n^p} \Psi_p^{-1} \quad (2.30)$$

2.4. The transformation matrices for nodal displacements and pore pressures

In SBFEM, the strain field formulation was given by wolf [31] as

$$\boldsymbol{\varepsilon}(\xi, \eta) = \mathbf{B}_1(\eta) \mathbf{u}(\xi)_{,\xi} + \frac{1}{\xi} \mathbf{B}_2(\eta) \mathbf{u}(\xi) \quad (2.31)$$

Substituting the displacement functions $\mathbf{u}(\xi)$ into Eq. (2.31), the strain field can be expressed in terms of \mathbf{u}_b as

$$\boldsymbol{\varepsilon}(\xi, \eta) = (\mathbf{B}_1(\eta) \Psi_u S_n + \mathbf{B}_2(\eta) \Psi_u) \xi^{-S_n-I} \Psi_u^{-1} \mathbf{u}_b \quad (2.32)$$

The matrix product before \mathbf{u}_b is defined as the so-called strain-displacement matrix $\mathbf{B}_u(\xi, \eta)$ in the following equations

$$\mathbf{B}_u(\xi, \eta) = (\mathbf{B}_1(\eta) \Psi_u S_n + \mathbf{B}_2(\eta) \Psi_u) \xi^{-S_n-I} \Psi_u^{-1} \quad (2.33)$$

where $\mathbf{B}_1(\eta)$ and $\mathbf{B}_2(\eta)$ are transformation coefficient matrices which have the following expression

$$\mathbf{B}_1(\eta) = \frac{1}{|J(\eta)|} \begin{bmatrix} y(\eta)_{,\eta} & 0 \\ 0 & -x(\eta)_{,\eta} \\ -x(\eta)_{,\eta} & y(\eta)_{,\eta} \end{bmatrix} \mathbf{N}_u(\eta) \quad (2.34)$$

$$\mathbf{B}_2(\eta) = \frac{1}{|J(\eta)|} \begin{bmatrix} -y(\eta) & 0 \\ 0 & x(\eta) \\ x(\eta) & -y(\eta) \end{bmatrix} \mathbf{N}_u(\eta)_{,\eta} \quad (2.35)$$

Similar to the transformation relation between strain and nodal displacements, the relationship between the pore pressure gradient of a point in a polygon element and nodal pore pressures can be derived from the following equations

$$\nabla p(\xi, \eta) = \mathbf{B}_1^p(\eta) \mathbf{p}(\xi)_{,\xi} + \frac{1}{\xi} \mathbf{B}_2^p(\eta) \mathbf{p}(\xi) \quad (2.36)$$

Substituting pore pressure functions $\mathbf{p}(\xi)$ into Eq. (2.36), the pore pressure gradient can be expressed in terms of \mathbf{p}_b as

$$\nabla p(\xi, \eta) = (\mathbf{B}_1^p(\eta) \Psi_p \mathbf{S}_n^p + \mathbf{B}_2^p(\eta) \Psi_p) \xi^{-S_n^p - I} \Psi_p^{-1} \mathbf{p}_b \quad (2.37)$$

The transformation matrix between pore pressure gradient $\nabla p(\xi, \eta)$ and nodal pressure \mathbf{p}_b can be given as

$$\mathbf{B}_p(\xi, \eta) = (\mathbf{B}_1^p(\eta) \Psi_p \mathbf{S}_n^p + \mathbf{B}_2^p(\eta) \Psi_p) \xi^{-S_n^p - I} \Psi_p^{-1} \quad (2.38)$$

where $\mathbf{B}_1^p(\eta)$ and $\mathbf{B}_2^p(\eta)$ are also the transformation coefficient matrices given as below

$$\mathbf{B}_1^p(\eta) = \frac{1}{|J(\eta)|} \begin{Bmatrix} y(\eta)_{,\eta} \\ -x(\eta)_{,\eta} \end{Bmatrix} \mathbf{N}_p(\eta) \quad (2.39)$$

$$\mathbf{B}_2^p(\eta) = \frac{1}{|J(\eta)|} \begin{Bmatrix} -y(\eta) \\ x(\eta) \end{Bmatrix} \mathbf{N}_p(\eta)_{,\eta} \quad (2.40)$$

3. The polygon scaled boundary equations for dynamic analysis of saturated soil

3.1. Generalized Biot's dynamic consolidation equations

Since Biot's dynamic consolidation theory was firstly presented in 1956, it has been widely used in dynamic problems related to the saturated porous media. Several forms of the equations were deduced by Zienkiewicz et al. [30], among which u - p form is a simple one which is precisely in most problems without high-frequency factors and is prone to be used in computation of large algebraic equations system and non-linear problems. In this paper, this u - p form equations are chosen as the governing equations.

The effective stress vector σ' can be expressed as below

$$\sigma' = \sigma + \alpha m p \quad (3.1a)$$

with

$$\mathbf{m} = \begin{Bmatrix} 1 \\ 1 \\ 0 \end{Bmatrix} \quad (3.1b)$$

where σ is the total stress vector and p is the pore pressure. α is a parameter related to the bulk modulus ratio of the solid skeleton to the solid particle.

The equilibrium equations of the solid-fluid mixture can be expressed as

$$\mathbf{L}^T(\sigma' - \alpha m p) - \rho \ddot{\mathbf{u}} + \rho \mathbf{b} = \mathbf{0} \quad (3.2a)$$

with

$$\sigma' = \mathbf{D} \epsilon = \mathbf{D} \mathbf{L} \mathbf{u} \quad (3.2b)$$

where ρ is the density of the mixture and \mathbf{b} is the body load vector. $\ddot{\mathbf{u}}$ is the acceleration vector of the solid skeleton and \mathbf{D} is the constitutive

matrix. \mathbf{u} is the displacement vector and ϵ is the strain vector. \mathbf{L} is the transformation matrix with the following form

$$\mathbf{L} = \begin{bmatrix} \frac{\partial}{\partial x} & 0 & \frac{\partial}{\partial y} \\ 0 & \frac{\partial}{\partial y} & \frac{\partial}{\partial x} \end{bmatrix}^T \quad (3.3)$$

The equilibrium equations of the fluid can be expressed as

$$-\nabla p - \mathbf{R} - \rho_f \ddot{\mathbf{u}} + \rho_f \mathbf{b} = \mathbf{0} \quad (3.4)$$

where \mathbf{R} are the viscous drag forces and ρ_f is density of the pore fluid. ∇ is the gradient operator with a form as

$$\nabla = \left\{ \frac{\partial}{\partial x} \quad \frac{\partial}{\partial y} \right\}^T \quad (3.5)$$

Darcy law can be expressed as

$$\mathbf{k} \mathbf{R} = \mathbf{w} \quad (3.6)$$

where \mathbf{k} is the permeability with the dimensions of $[\text{length}]^3[\text{time}]^2/[\text{mass}]$ and \mathbf{w} is the average velocity vector of the percolating fluid.

The mass conservation equation can be described as

$$\nabla^T \mathbf{w} + \alpha \nabla^T \dot{\mathbf{u}} + \frac{\dot{p}}{Q} = 0 \quad (3.7)$$

where n is the porosity and $\dot{\mathbf{u}}$ is the velocity vector. \dot{p} is the first order derivative of pore pressure with respect to time. And Q is a modulus defined as below

$$\frac{1}{Q} = \frac{n}{K_f} + \frac{\alpha - n}{K_s} \quad (3.8)$$

where K_f is the bulk modulus of the fluid and K_s is the bulk modulus of the solid particle.

Substituting Eq. (3.4) and Eq. (3.6) into mass conservation equation Eq. (3.7) gives the following expression

$$-\nabla^T \mathbf{k} \nabla p - \rho_f \nabla^T \mathbf{k} \ddot{\mathbf{u}} + \rho_f \nabla^T \mathbf{k} \mathbf{b} + \alpha \nabla^T \dot{\mathbf{u}} + \frac{\dot{p}}{Q} = 0 \quad (3.9)$$

Eq. (3.2a) and Eq. (3.9) are the so-called u - p form dynamic consolidation equations of saturated porous media.

3.2. The derivation of the scaled boundary polygon equations for dynamic analysis of saturated soil

The spatial discretization involving variables \mathbf{u} and p is achieved by displacement shape functions given in Eq. (2.17) and pore pressure shape functions given in Eq. (2.30). The Galerkin method utilizing the shape functions as the test functions and Green formula are applied to the equilibrium equations given in Eq. (3.2a), which transforms the equations into the following form

$$\mathbf{M} \ddot{\mathbf{u}} + \mathbf{K} \dot{\mathbf{u}} - \mathbf{Q}_{sf} \dot{\mathbf{p}} - \mathbf{f}^1 = \mathbf{0} \quad (3.10)$$

Introducing Rayleigh damping into Eq. (3.10) gives

$$\mathbf{M} \ddot{\mathbf{u}} + \mathbf{C} \dot{\mathbf{u}} + \mathbf{K} \dot{\mathbf{u}} - \mathbf{Q}_{sf} \dot{\mathbf{p}} - \mathbf{f}^1 = \mathbf{0} \quad (3.11)$$

where $\ddot{\mathbf{u}}$, $\dot{\mathbf{u}}$ and \mathbf{u} are the nodal displacement vector, velocity vector and acceleration vector, respectively. $\dot{\mathbf{p}}$ is the nodal pore pressure vector and \mathbf{f}^1 is the nodal external load vector. \mathbf{M} is the mass matrix and \mathbf{C} is the damping matrix. \mathbf{K} is the stiffness matrix and \mathbf{Q}_{sf} is the solid-fluid coupling matrix. The vectors and coefficient matrices mentioned above have the following expressions

$$\mathbf{M} = \iint_{\Omega} \Phi_u(\xi, \eta)^T \rho \Phi_u(\xi, \eta) d\Omega \quad (3.12)$$

$$\mathbf{K} = \iint_{\Omega} \mathbf{B}_u(\xi, \eta)^T \rho \mathbf{B}_u(\xi, \eta) d\Omega \quad (3.13)$$

$$\mathbf{C} = \alpha \mathbf{M} + \beta \mathbf{K} \quad (3.14)$$

$$\mathbf{Q}_{sf} = \iint_{\Omega} \mathbf{B}_u^T(\xi, \eta) \alpha \mathbf{m} \Phi_p(\xi, \eta) d\Omega \quad (3.15)$$

$$\mathbf{f}^1 = \iint_{\Omega} \Phi_u(\xi, \eta)^T \rho b d\Omega + \iint_{\Gamma_t} \Phi_u(\xi, \eta)^T T d\Gamma \quad (3.16)$$

where Φ_u are the displacement shape functions given in Eq. (2.17) and Φ_p are the pore pressure shape functions given in Eq. (2.30). $\mathbf{B}_u(\xi, \eta)$ is the strain-displacement transformation matrix defined in Eq. (2.33).

Applying Galerkin method and Green formula to the mass conservation equation given in Eq. (3.9), it is transformed into the following form

$$\mathbf{Q}_{fs} \dot{\mathbf{u}} + \mathbf{S} \dot{\mathbf{p}} + \mathbf{H} \bar{\mathbf{p}} - \mathbf{f}^2 = \mathbf{0} \quad (3.17)$$

where \mathbf{Q}_{fs} is the fluid–solid coupling matrix and \mathbf{S} is the compression matrix. \mathbf{H} is the penetration matrix and \mathbf{f}^2 is the nodal external load vector corresponding to fluid. $\dot{\mathbf{p}}$ is the first order derivative of the nodal pressure vector. The explicit expressions of the coefficient matrices and vectors mentioned above are as follows

$$\mathbf{H} = \iint_{\Omega} \mathbf{B}_p(\xi, \eta)^T \mathbf{k} \mathbf{B}_p(\xi, \eta) d\Omega \quad (3.18)$$

$$\mathbf{S} = \iint_{\Omega} \Psi_p(\xi, \eta)^T \frac{1}{Q} \Psi_p(\xi, \eta) d\Omega \quad (3.19)$$

$$\mathbf{Q}_{fs} = \mathbf{Q}_{sf}^T = \iint_{\Omega} \Phi_p^T(\xi, \eta) \alpha \mathbf{m}^T \mathbf{B}_u(\xi, \eta) d\Omega \quad (3.20)$$

$$\mathbf{f}^2 = \iint_{\Omega} \mathbf{B}_p(\xi, \eta)^T \mathbf{k} \rho_f b d\Omega + \int_{\Gamma_w} \Psi_p(\xi, \eta)^T q d\Gamma \quad (3.21)$$

$\mathbf{B}_p(\xi, \eta)$ used in the above equations is a transformation matrix between pore pressure gradient and nodal pore pressures and is given in Eq. (2.38).

Eq. (3.11) and Eq. (3.17) are ordinary differential equations with respect to time. The solution of the equations requires discretization in time, which can be achieved by the Generalized Newmark method [30]. The recurrence relation between the unknown variables at time station t_n and that at time station $t_n + \Delta t$ is

$$\begin{aligned} \ddot{\mathbf{u}}_{n+1} &= \ddot{\mathbf{u}}_n + \Delta \ddot{\mathbf{u}}_n \\ \dot{\mathbf{u}}_{n+1} &= \dot{\mathbf{u}}_n + \ddot{\mathbf{u}}_n \Delta t + \beta_1 \Delta \ddot{\mathbf{u}}_n \Delta t \\ \bar{\mathbf{u}}_{n+1} &= \bar{\mathbf{u}}_n + \dot{\mathbf{u}}_n \Delta t + \frac{1}{2} \ddot{\mathbf{u}}_n \Delta t^2 + \frac{1}{2} \beta_2 \Delta \ddot{\mathbf{u}}_n \Delta t^2 \end{aligned} \quad (3.22a)$$

and

$$\begin{aligned} \dot{\mathbf{p}}_{n+1} &= \dot{\mathbf{p}}_n + \Delta \dot{\mathbf{p}}_n \\ \bar{\mathbf{p}}_{n+1} &= \bar{\mathbf{p}}_n + \dot{\mathbf{p}}_n \Delta t + \bar{\beta}_1 \Delta \dot{\mathbf{p}}_n \Delta t \end{aligned} \quad (3.22b)$$

where β_1 , β_2 and $\bar{\beta}_1$ are constants ranging from 0 to 1. $\ddot{\mathbf{u}}_{n+1}$, $\dot{\mathbf{u}}_{n+1}$ and $\bar{\mathbf{u}}_{n+1}$ are the acceleration, velocity and displacement variables of the n th step. $\dot{\mathbf{p}}_{n+1}$ and $\bar{\mathbf{p}}_{n+1}$ are the first order derivative of pore pressure and pressure of n th step.

Eq. (3.11) and Eq. (3.17) at time station t_{n+1} can be written as

$$\mathbf{M}_{n+1} \ddot{\mathbf{u}}_{n+1} + \mathbf{C}_{n+1} \dot{\mathbf{u}}_{n+1} + \mathbf{K}_{n+1} \bar{\mathbf{u}}_{n+1} - \mathbf{Q}_{sf n+1} \bar{\mathbf{p}}_{n+1} - \mathbf{f}_{n+1}^1 = \mathbf{0} \quad (3.23)$$

$$\mathbf{Q}_{fs n+1} \dot{\mathbf{u}}_{n+1} + \mathbf{S}_{n+1} \dot{\mathbf{p}} + \mathbf{H}_{n+1} \bar{\mathbf{p}}_{n+1} - \mathbf{f}_{n+1}^2 = \mathbf{0} \quad (3.24)$$

Inserting Eq. (3.22a) and Eq. (3.22b) into Eq. (3.23) and Eq. (3.24) yields an equation set where $\Delta \dot{\mathbf{p}}_n$ and $\Delta \ddot{\mathbf{u}}_n$ are unknown variables and which can be written as

$$\begin{aligned} \Psi_{n+1}^1 &= \mathbf{M}_{n+1} \Delta \ddot{\mathbf{u}}_n + \mathbf{C}_{n+1} \beta_1 \Delta t \Delta \ddot{\mathbf{u}}_n + \frac{1}{2} \mathbf{K}_{n+1} \beta_2 \Delta t^2 \Delta \ddot{\mathbf{u}}_n \\ &\quad - \mathbf{Q}_{sf n+1} \bar{\beta}_1 \Delta t \Delta \dot{\mathbf{p}}_n - \mathbf{F}_{n+1}^1 = \mathbf{0} \end{aligned} \quad (3.25)$$

$$\Psi_{n+1}^2 = \mathbf{Q}_{fs n+1} \beta_1 \Delta t \ddot{\mathbf{u}}_n + \mathbf{S}_{n+1} \Delta \dot{\mathbf{p}}_n + \mathbf{H}_{n+1} \bar{\beta}_1 \Delta t \Delta \dot{\mathbf{p}}_n - \mathbf{F}_{n+1}^2 = \mathbf{0} \quad (3.26)$$

where \mathbf{F}_{n+1}^1 and \mathbf{F}_{n+1}^2 can be evaluated explicitly from the information available at time station t_n

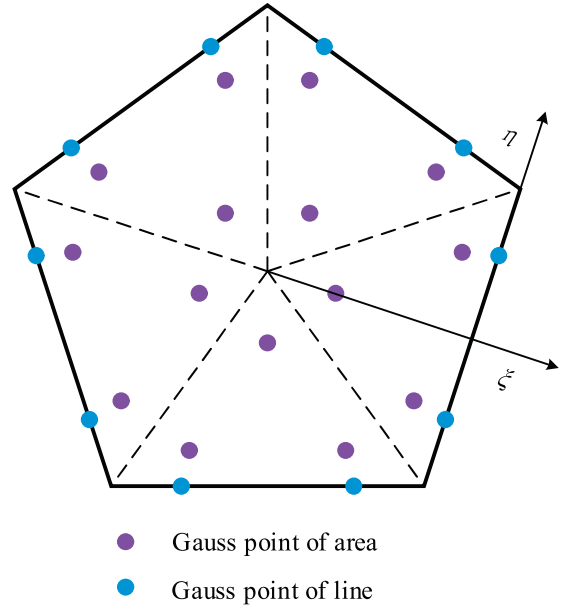


Fig. 3.1. Location of Gaussian points within a polygon element.

$$\begin{aligned} \mathbf{F}_{n+1}^1 &= \mathbf{f}_{n+1}^1 - \mathbf{M}_{n+1} \ddot{\mathbf{u}}_n - \mathbf{C}_{n+1} \dot{\mathbf{u}}_n - \mathbf{C}_{n+1} \Delta t \ddot{\mathbf{u}}_n - \mathbf{K}_{n+1} \bar{\mathbf{u}}_n \\ &\quad - \mathbf{K}_{n+1} \Delta t \dot{\mathbf{u}}_n - \frac{1}{2} \mathbf{K}_{n+1} \Delta t^2 \ddot{\mathbf{u}}_n + \mathbf{Q}_{sf n+1} \bar{\mathbf{p}}_n + \mathbf{Q}_{sf n+1} \Delta t \dot{\mathbf{p}}_n \end{aligned} \quad (3.27)$$

$$\mathbf{F}_{n+1}^2 = \mathbf{f}_{n+1}^2 - \mathbf{Q}_{fs n+1} \dot{\mathbf{u}}_n - \mathbf{Q}_{fs n+1} \Delta t \ddot{\mathbf{u}}_n - \mathbf{S}_{n+1} \dot{\mathbf{p}}_n - \mathbf{H}_{n+1} \bar{\mathbf{p}}_n - \mathbf{H}_{n+1} \Delta t \dot{\mathbf{p}}_n \quad (3.28)$$

The equations in Eq. (3.25) and Eq. (3.26) can be solved by Newton Raphson procedure.

3.3. The evaluation of the coefficient matrix

The conventional finite element theory is used to evaluate the coefficient matrices of the polygon scaled boundary equations in the presented method which is proposed by Chen et al. [32]. A major advantage of this method is that the material nonlinear can be taken into consideration.

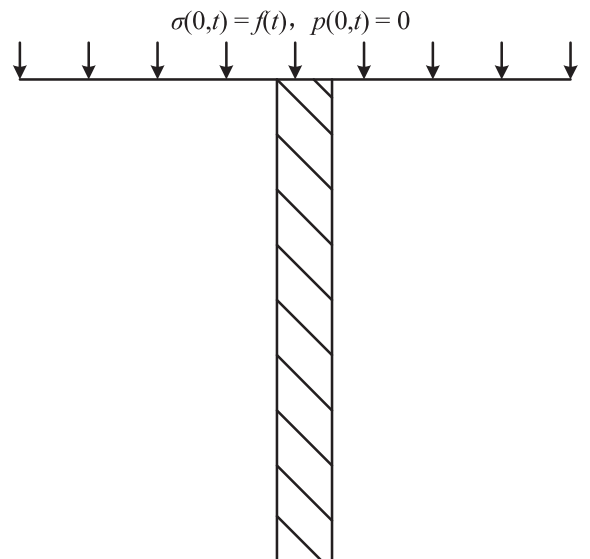


Fig. 5.1. Sketch for saturated elastic half space.

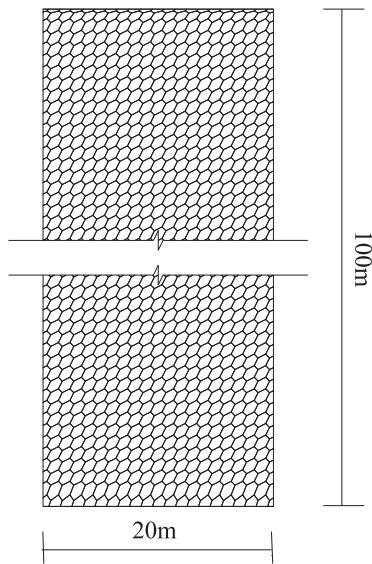


Fig. 5.2. Polygon mesh for saturated elastic half space.

Table 5.1

Parameters corresponding to Boer et al. [2].

E (MPa)	ν	n	ρ_s (Kg/m ³)	ρ_f (Kg/m ³)	K_s (Pa)	K_f (Pa)	k (m/s)
30	0.2	0.333	2670	1000	∞	∞	0.01

Table 5.2

Parameters corresponding to Simon et al. [3].

E (Pa)	ν	n	ρ_s (Kg/m ³)	ρ_f (Kg/m ³)	K_s (Pa)	K_f (Pa)	k (m ³ s/Kg)
3000	0.2	0.333	0.3110	0.2977	∞	39,990	0.004883

This method will be concisely described here. In a polygon, a sector covered by a line element is taken as a triangular element and three Gaussian integration points are introduced into this element. The locations of the points are determined according to the integration rule of triangular element and their positions in a polygon are shown in Fig. 3.1. The Gaussian points of the line are used to calculate the SBFEM coefficients, and the Gaussian points of the area are used for integration for the coefficient matrices of the scaled boundary polygon equations derived in Section 3.2. Any coefficient matrix of a polygon element can be calculated by adding the integration over every triangular element in the polygon. For example, the stiffness matrix of a polygon element

with n -side can be calculated as

$$\begin{aligned} \mathbf{K} &= \iint_{\Omega} \mathbf{B}_u(\xi, \eta)^T \mathbf{D} \mathbf{B}_u(\xi, \eta) d\Omega \\ &= \sum_{i=1}^{3n} w_i |\mathbf{J}_i(\xi, \eta)| \mathbf{B}_u^i(\xi, \eta)^T \mathbf{D}_i \mathbf{B}_u^i(\xi, \eta) \end{aligned} \quad (3.29)$$

where w_i is the weight coefficient of the i th Gauss point in the polygon element and $\mathbf{B}_u^i(\xi, \eta)$ is the strain–displacement transformation matrix of the i th Gauss point in the polygon element. \mathbf{D} is the elastic constitutive matrix of the i th Gauss point, and can be replaced by an elasto-plastic constitutive matrix \mathbf{D}_{ep} in nonlinear analysis which makes the proposed method competent in both elastic and elastic-plastic problems.

4. Polygon scaled boundary procedure for dynamic analysis of saturated soil

Based on the proposed method, a new type of scaled boundary polygon element is developed with object-oriented C++ programming language and integrated into the windows software GEODYNA developed by the first author. By introducing the parallel computing method, this software is competent for elasto-plastic problem with millions of DOFs.

5. Numerical examples

5.1. A saturate elastic half space subjected to a uniform cyclic loading

5.1.1. Model and parameters

A saturated elastic half space subjected to a uniform surface cyclic loading is shown in Fig. 5.1. The surface of the half space is free to drain. Actually, it is a one-dimensional transit response problem of infinite column. In order to validate the accuracy of the presented method, numerical simulations are conducted to this problem with a polygon mesh shown in Fig. 5.2. In order to decrease the influence of boundary effect, the vertical length is set as 100 m. The displacement at the bottom and the horizontal displacement of the side surface are fixed, and the pore pressure at the surface is set as zero while the side surface is set as impermeable, which corresponds to the problem to be modeled.

The analytical solution of this problem was given by Boer et al. [2], where the solid particle and fluid are both considered as incompressible material. In addition, another analytical solution of this problem was given by Simon et al. [3], where the solid particle is treated as incompressible material while the fluid is treated as compressible material. For the first condition considered by Boer, the material parameters are listed in Table 5.1 and the surface loading function is $f(t) = 3000(1 - \cos 75t)$ Pa. For the second condition considered by Simon, the material parameters are listed in Table 5.2 and the surface loading function is $f(t) = \sigma_0 \sin 62.83t$ Pa.

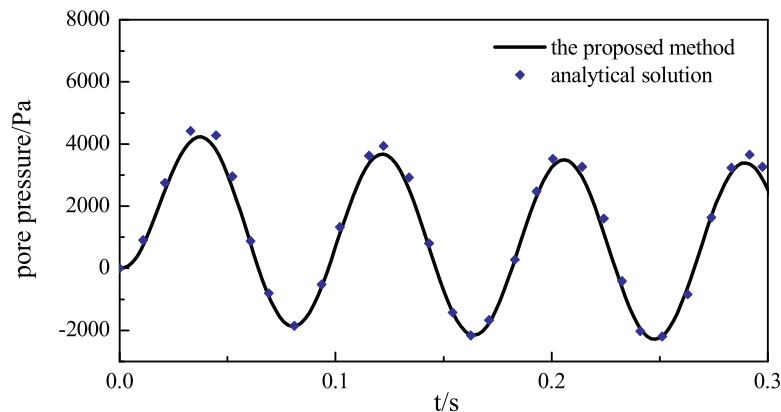


Fig. 5.3. Pore pressure of the location 1 m below the surface of the elastic half space.

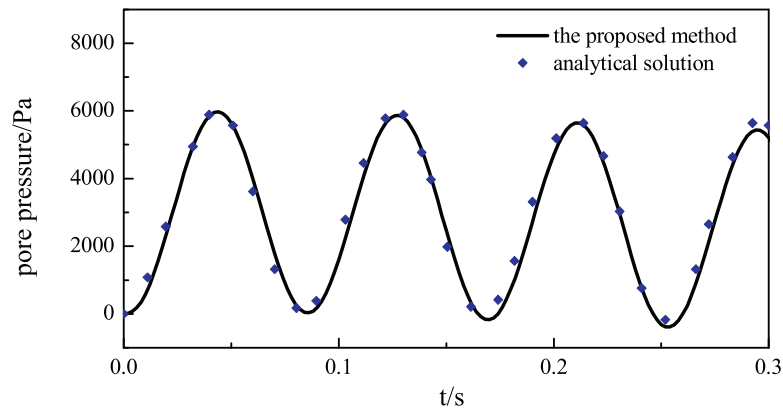


Fig. 5.4. Pore pressure of the location 6 m below the surface of the elastic half space.

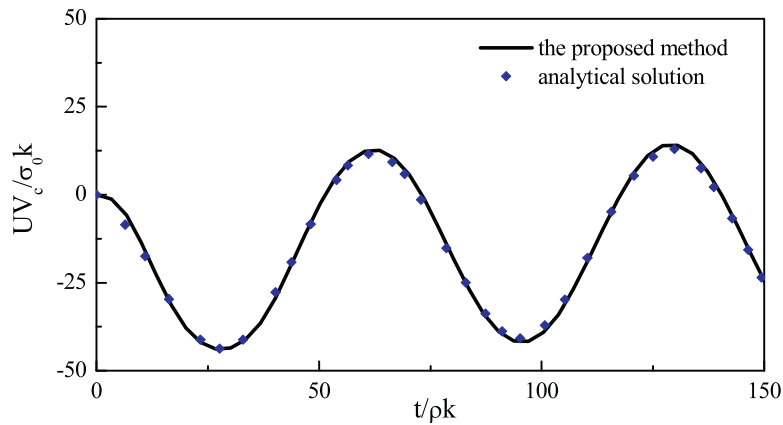


Fig. 5.5. Non-dimensional vertical displacement at the surface of the elastic half space.

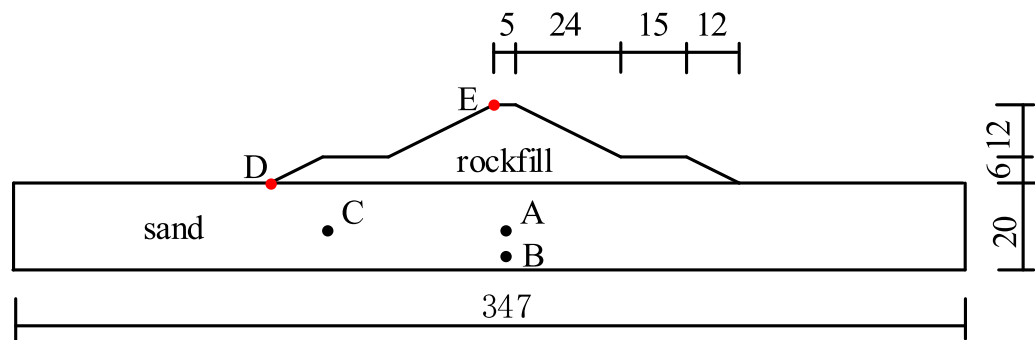


Fig. 5.6. Sketch for a rockfill breakwater built on sand foundation (units: m).

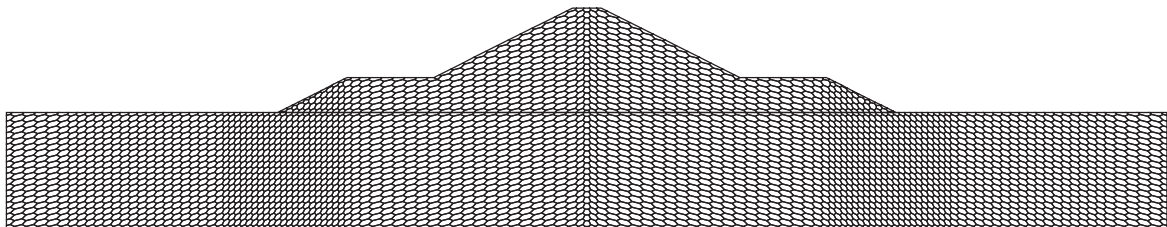


Fig. 5.7. Polygon scaled boundary finite element mesh of the breakwater.

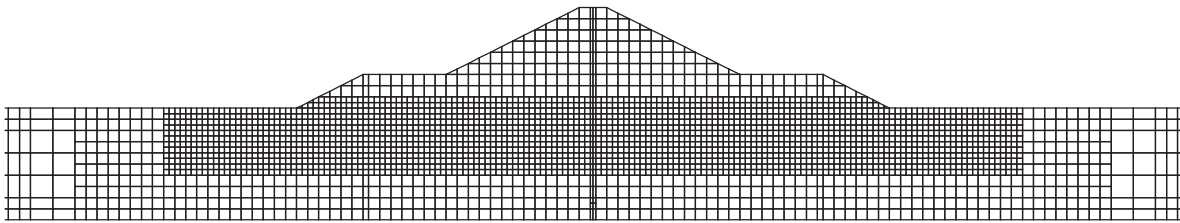


Fig. 5.8. Quadtree mesh of the breakwater.

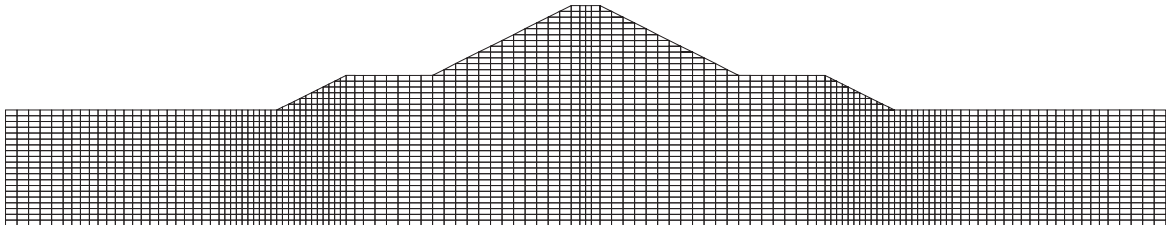


Fig. 5.9. Finite element mesh of the breakwater.

Table 5.3
Parameters of generalized plastic model of sand.

ρ_s (kg/m ³)	ρ_f (kg/m ³)	n	M_f	M_g	α_f	α_g	β_0	β_1
2670	1000	0.42	1.03	1.15	0.45	0.45	4.2	0.2
H_{10}	H_{u0} (Pa)	γ_{Hu}	γ_{Dm}	K_0 (Pa)	G_0 (Pa)			
600	4e6	2	0	7.7e5	1.15e6			

Table 5.4
Parameters of generalized plastic model of rockfill.

ρ (kg/m ³)	M_f	M_g	α_f	α_g	β_0	β_1	H_{10}	H_{u0}
1800	0.7	1.72	0.411	0.3	60	0.053	2450	1600
γ_{Hu}	γ_{Dm}	m_s	m_v	m_l	m_u	γ_d	K_0	G_0
5	30	0.8	0.8	0.14	0.5	20	1000	800

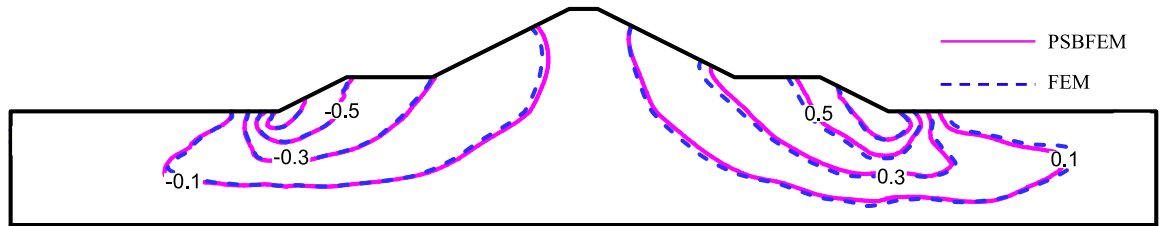
5.1.2. Numerical results

For the condition considered by Boer, the pore pressure result at the location 1 m below the surface of the half space is shown in Fig. 5.3 and the pore pressure result at the location 6 m underneath the surface of the half space is shown in Fig. 5.4. The results correspond well with the analytical solutions which indicates the proposed method is capable for dynamic analysis of saturated elastic porous media. For the condition considered by Simon, the non-dimensional vertical displacement on the surface of the elastic half space is shown in Fig. 5.5 where the numerical result shows a good correspondence with the analytical solution as well.

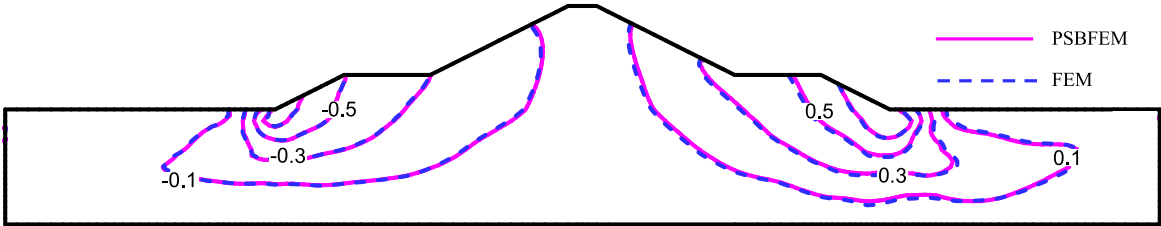
5.2. A liquefaction analysis for a rockfill breakwater erected on saturated sand foundation

5.2.1. Model and parameters

To investigate the applicability of the newly developed polygon scaled boundary method in simulating nonlinear dynamic problems included saturated soil, the liquefaction analysis of a breakwater erected on a saturated sand foundation is conducted using both the presented method and FEM. The geometry model of this problem is shown in Fig. 5.6. The SBFEM discretized with polygon mesh and quadtree mesh is

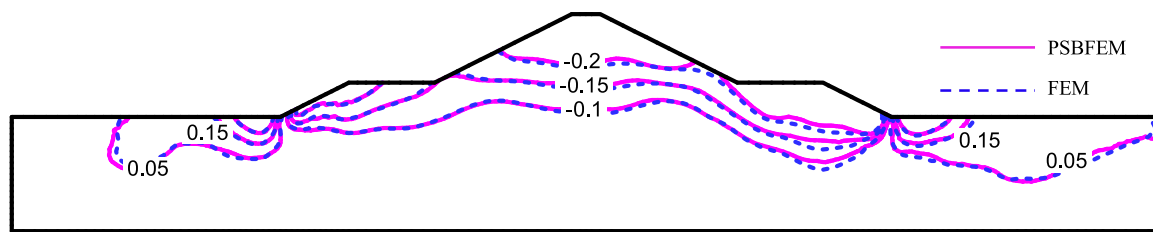


(a) Comparison of the results computed by FEM and PSBFEM discretized with polygon mesh

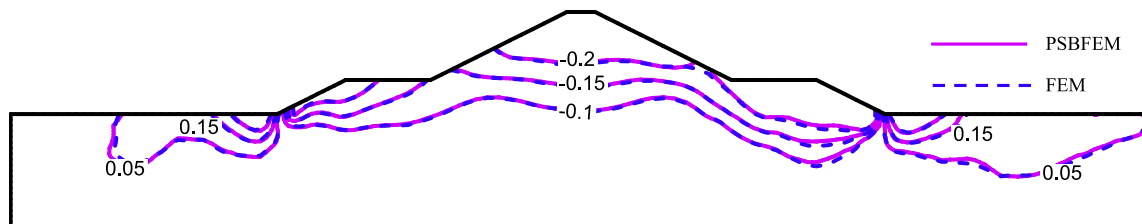


(b) Comparison of the results computed by FEM and PSBFEM discretized with quadtree mesh

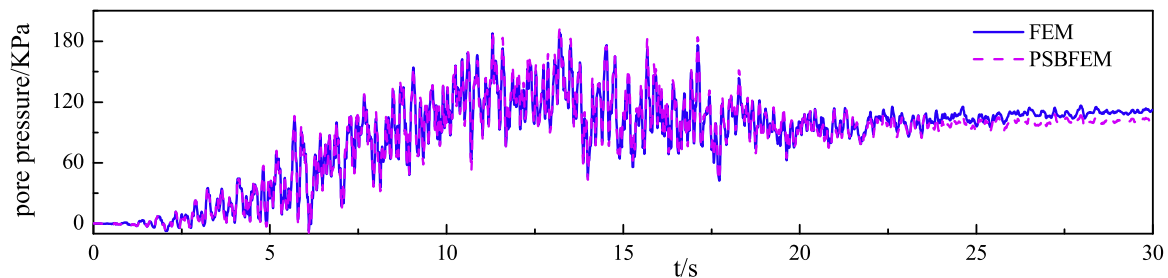
Fig. 5.10. Horizontal displacement distribution of the breakwater after earthquake (units: m).



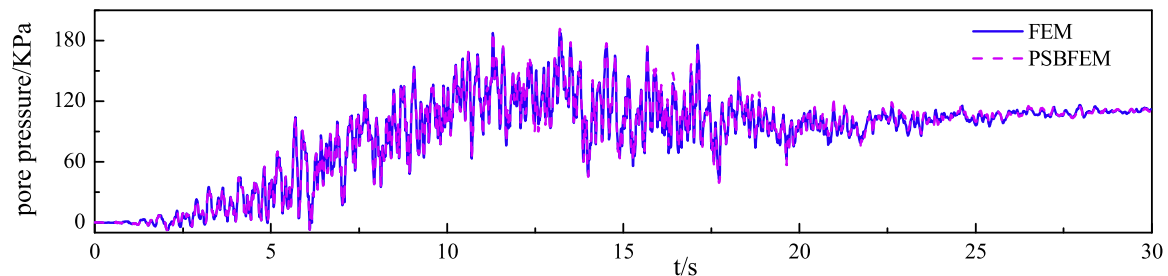
(a) Comparison of the results computed by FEM and PSBFEM discretized with polygon mesh



(b) Comparison of the results computed by FEM and PSBFEM discretized with quadtree mesh

Fig. 5.11. Vertical displacement distribution of the breakwater after earthquake (units: m).

(a) Comparison of the results computed by FEM and PSBFEM discretized with polygon mesh



(b) Comparison of the results computed by FEM and PSBFEM discretized with quadtree mesh

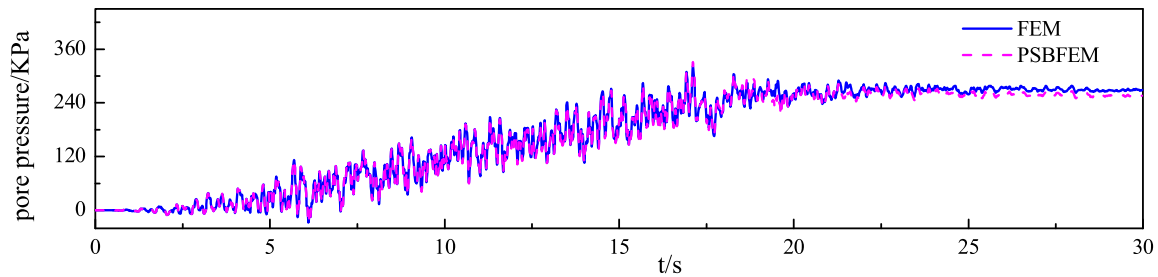
Fig. 5.12. Pore pressure time history of location A.

shown in Figs. 5.7 and 5.8, respectively. The FEM mesh discretized with quadrilateral isoparametric elements is shown in Fig. 5.9. The boundary constraint conditions are set as that the displacement at the bottom of the sand foundation is fixed and the pore pressure at the surface of the sand foundation is fixed. A horizontal ground motion with a peak acceleration of 0.2 g and a vertical ground motion with a peak acceleration of 0.133 g are input. The sand and the rockfill are modeled with modified generalized plastic model [33–36], whose parameters are listed in Table 5.3 and Table 5.4, respectively.

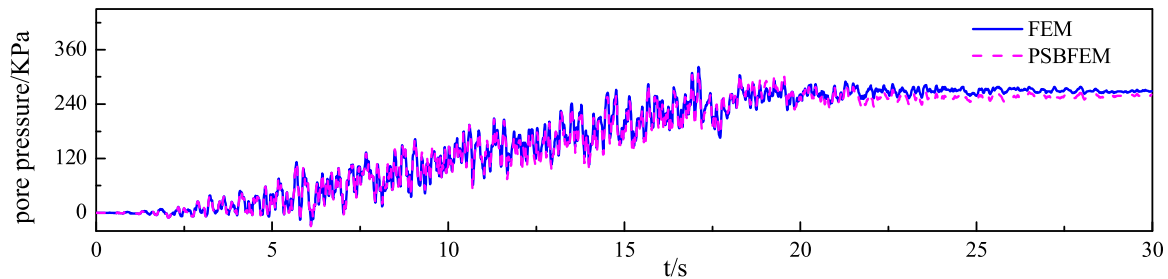
5.2.2. Numerical results

The displacements after the seismic calculated with SBFEM using polygon mesh and FEM are compared in Fig. 5.10(a) and 5.11(a). The results of the two methods correspond well with each other and only minor difference can be found in both spatial distribu-

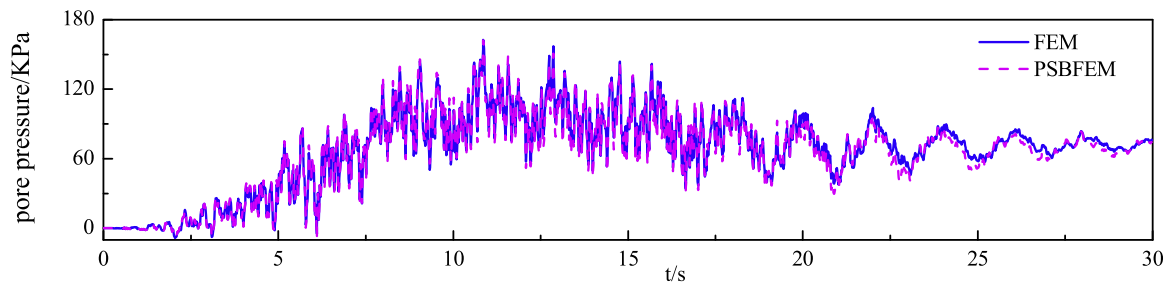
tion and magnitude. A, B and C are three pore pressure supervision points in the sand foundation shown in Fig. 5.6. The time histories of the pore pressure of these three points obtained with FEM and PSBFEM discretized with polygon mesh are compared in Fig. 5.12(a) to Fig. 5.14(a), where a good agreement is achieved in both trend and magnitude. D and E are two displacement supervision points shown in Fig. 5.6. The horizontal displacement time history of point D and the vertical displacement time history of point E obtained by FEM and PSBFEM discretized with polygon mesh are compared in Fig. 5.15(a) and Fig. 5.16(a), where the results of the two methods correspond well. The displacement distribution of the breakwater calculated by FEM and PSBFEM discretized with quadtree mesh is compared in Fig. 5.10(b) and Fig. 5.11(b). The results calculated with quadtree mesh correspond well with that calculated with FEM. The pressure histories of point A, and



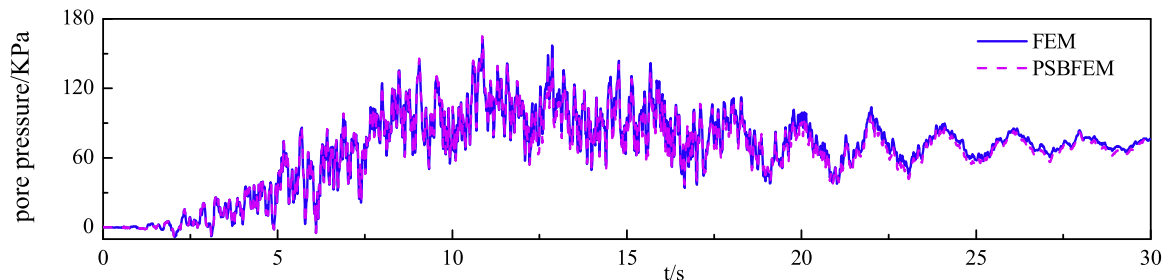
(a) Comparison of the results computed by FEM and PSBFEM discretized with polygon mesh



(b) Comparison of the results computed by FEM and PSBFEM discretized with quadtree mesh

Fig. 5.13. Pore pressure time history of location B.

(a) Comparison of the results computed by FEM and PSBFEM discretized with polygon mesh



(b) Comparison of the results computed by FEM and PSBFEM discretized with quadtree mesh

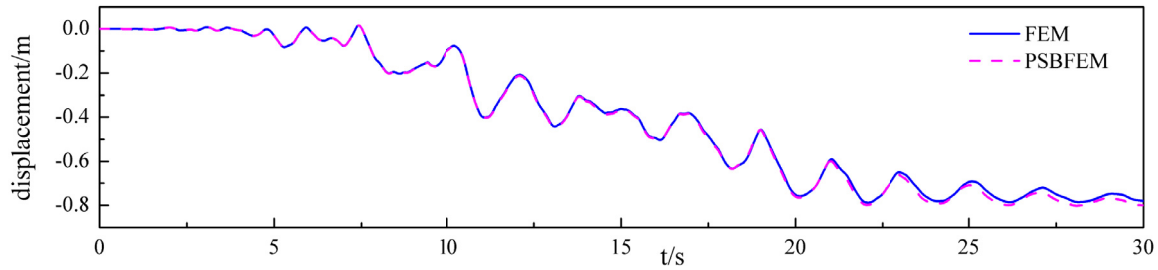
Fig. 5.14. Pore pressure time history of location C.

C and the displacement histories of point D and E calculated by FEM and PSBFEM discretized with quadtree mesh are compared in Fig. 5.12(b) to 5.16(b), respectively. The results also achieve a good agreement. The computation time of FEM is 50.2 min, while the computation time of PSBFEM discretized with quadtree mesh is 65.2 min which is slight higher than that of FEM. The good agreement of the results obtained by FEM and PSBFEM indicates that the proposed method is reliable and accurate in both polygon mesh and quadtree mesh. The SBFEM which treat a quadrilateral element with hanging nodes as a polygon element is highly compatible with quadtree decomposition without any additional efforts. With the help of quadtree mesh, the mesh generation is faster and more automatic than FEM which will significantly reduce the workload in pre-

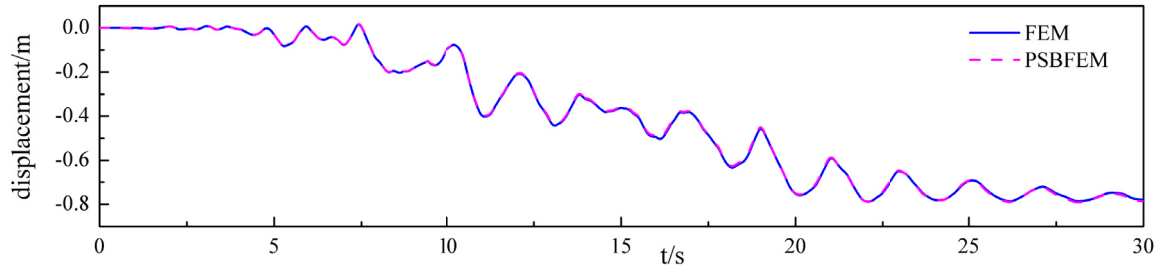
processing. The good correspondence of the results derived from FEM and PSBFEM indicates that the presented method is effective in modeling nonlinear dynamic analysis of saturated soil and the advantages in mesh generation make it highly applicable to engineering practice.

6. Conclusions

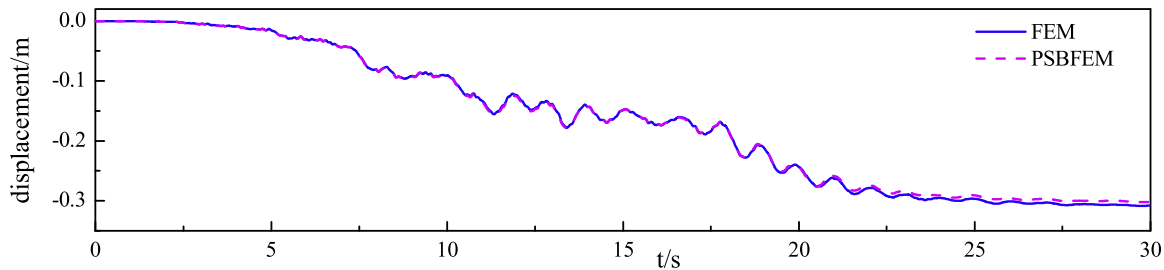
In this paper, the PSBFEM is extended to solve nonlinear dynamic analysis of saturated soil based on generalized Biot's dynamic consolidation theory. The displacement shape functions and the pore pressure shape functions are constructed from the elastic static theory and steady-state seepage theory within the SBFEM framework respectively, which



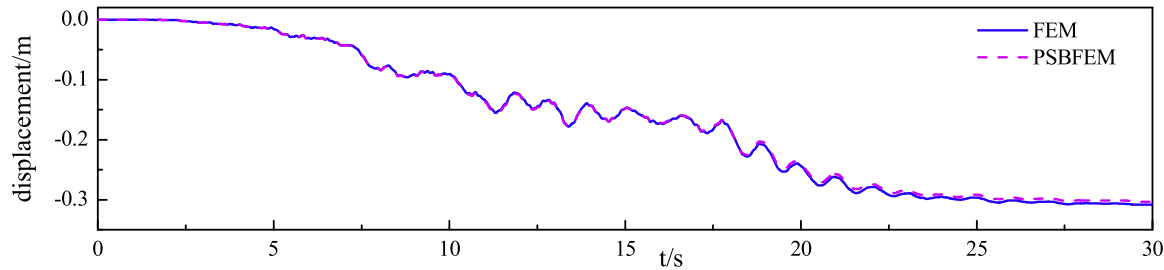
(a) Comparison of the results computed by FEM and PSBFEM discretized with polygon mesh



(b) Comparison of the results computed by FEM and PSBFEM discretized with quadtree mesh

Fig. 5.15. Horizontal displacement time history of location D.

(a) Comparison of the results computed by FEM and PSBFEM discretized with polygon mesh



(b) Comparison of the results computed by FEM and PSBFEM discretized with quadtree mesh

Fig. 5.16. Vertical displacement time history of location E.

can be computed with the Gauss points of line. Then the scaled boundary polygon equations for dynamic analysis of saturated soil is obtained through the detailed derivation. Nonlinearity is taken into consideration in the presented method by introducing Gauss points of area into each subdomain.

The case of a saturated elastic half space subjected to a uniform cyclic dynamic loading is conducted and simulated firstly. Good agreement is obtained after the comparisons of the simulated results including displacement and pore pressure with exacted solution. Moreover, a liquefaction analysis for a breakwater based on generalized plastic model is subsequently conducted and solved by using both FEM and the proposed method with polygon mesh and quadtree mesh for the purpose of further model assessment. The spatial distribution and time histories

of displacement and pore pressure are compared. The results of the two methods match quite well.

The results of this study release that the polygon scale boundary element method can be successfully applied in saturated elastic-plastic soil area. The highly flexibility in modeling complex geometry, automatic mesh generation and fast mesh reconstruction is believed to make the proposed method a competitive alternative in large deformation analysis of saturated soil.

Acknowledgments

This work was supported by National Key R&D Program of China (2017YFC0404900) and the National Natural Science Foundation of

China (Grant Nos. 51779034, 51678113). This financial support is gratefully acknowledged.

References

- [1] Biot MA. Theory of propagation of elastic waves in a fluid-saturated porous solid. I. Low-frequency range.. *J Acoust Soc Am* 1956;28(2):179–91.
- [2] Boer RD, Ehlers W, Liu Z. One-dimensional transient wave propagation in fluid-saturated incompressible porous media. *Arch Appl Mech* 1993;63(1):59–72.
- [3] Simon BR, Zienkiewicz OC, Paul DK. An analytical solution for the transient response of saturated porous elastic solids. *Int J Numer Anal Methods Geomech* 1984;8(4):381–98.
- [4] Gajo A, Mongiovi L. An analytical solution for the transient response of saturated linear elastic porous media. *Int J Numer Anal Methods Geomech* 1995;19(6):399–13.
- [5] Schanz M, Cheng AHD. Wave propagation in a one-dimensional poroelastic column. *Acta Mech* 2000;145(1–4):1–18.
- [6] Ghaboussi J, Wilson EL. Variation formulation of dynamics of fluid-saturated porous elastic solids. *J Eng Mech Div* 1972;98(4):947–63.
- [7] Zienkiewicz OC, Shiomi T. Dynamic behaviour of saturated porous media; the generalized Biot formulation and its numerical solution. *Int J Numer Anal Methods Geomech* 1984;8(1):71–96.
- [8] Göransson P. A 3-D, symmetric, finite element formulation of the Biot equations with application to acoustic wave propagation through an elastic porous medium. *Int J Numer Methods Eng* 2015;41(1):167–92.
- [9] Chen J, Dargush GF. Boundary element method for dynamic poroelastic and thermoelastic analyses. *Int J Solids Struct* 1995;32(15):2257–78.
- [10] Wolf JP, Song C. The scaled boundary finite-element method—a primer: derivations. *Comput Struct* 2000;78(1):191–10.
- [11] Song C, Wolf JP. The scaled boundary finite-element method—a primer: solution procedures. *Comput. Struct.* 2000;78(1):211–25.
- [12] Song C, Wolf JP. The scaled boundary finite-element method—alias consistent infinitesimal finite-element cell method—for elastodynamics. *Comput Methods Appl Mech Eng* 1997;147(3–4):329–55.
- [13] Natarajan S, Ooi ET, Chiong I, Song C. Convergence and accuracy of displacement based finite element formulations over arbitrary polygons: Laplace interpolants, strain smoothing and scaled boundary polygon formulation. *Finite Elem Anal Des* 2014;85(4):101–22.
- [14] Bazyar MH, Song C. A continued-fraction-based high-order transmitting boundary for wave propagation in unbounded domains of arbitrary geometry. *Int J Numer Methods Eng* 2008;74(2):209–37.
- [15] Liu J, Lin G. A scaled boundary finite element method applied to electrostatic problems. *Eng Anal Bound Elem* 2012;36(12):1721–32.
- [16] Yang Z. Fully automatic modelling of mixed-mode crack propagation using scaled boundary finite element method. *Eng Fract Mech* 2006;73(12):1711–31.
- [17] Liu J, Zhang P, Lin G, Wang W, Lu S. High order solutions for the magneto-electro-elastic plate with non-uniform materials. *Int J Mech Sci* 2016;115:532–51.
- [18] Liu J, Lin G, Li J. Short-crested waves interaction with a concentric cylindrical structure with double-layered perforated walls. *Ocean Eng* 2012;40(1):76–90.
- [19] Lu S, Liu J, Lin G, Wang W. Time-domain analyses of the layered soil by the modified scaled boundary finite element method. *Struct Eng Mech* 2015;55(5):1055–86.
- [20] Li P, Liu J, Lin G, Zhang P, Yang G. A NURBS-based scaled boundary finite element method for the analysis of heat conduction problems with heat fluxes and temperatures on side-faces. *Int J Heat Mass Transfer* 2017;113:764–79.
- [21] Lin G, Pang L, Hu Z, Zhang Y. Improving accuracy and efficiency of stress analysis using scaled boundary finite elements. *Eng Anal Bound Elem* 2016;67:26–42.
- [22] Ooi ET, Song C, Tin-Loi F. A scaled boundary polygon formulation for elasto-plastic analyses. *Comput Methods Appl Mech Eng* 2014;268(1):905–37.
- [23] Chiong I, Song C. Development of polygon elements based on the scaled boundary finite element method; 2010. 012226.
- [24] Ooi ET, Song C, Tin-Loi F, Yang Z. Polygon scaled boundary finite elements for crack propagation modelling. *Int J Numer Methods Eng* 2012;91(3):319–42.
- [25] Ooi ET, Natarajan S, Song C, Ooi EH. Crack propagation modelling in concrete using the scaled boundary finite element method with hybrid polygon–quadtree meshes. *Int J Fract* 2016;203(1):1–23.
- [26] Dai S, Augarde C, Du C, Chen D. A fully automatic polygon scaled boundary finite element method for modelling crack propagation. *Eng Fract Mech* 2015;133:163–78.
- [27] Bao Y, Zhong H, Lin G. Seismic fracture simulation of gravity dam based on polygon scaled boundary finite elements. *Water Resour Power* 2015;4:72–5.
- [28] Chiong I, Ooi ET, Song C, Tin-Loi F. Scaled boundary polygons with application to fracture analysis of functionally graded materials. *Int J Numer Methods Eng* 2014;98(8):562–89.
- [29] Luo T, Ooi ET, Chan AHC, Fu SJ. The combined scaled boundary finite-discrete element method: Grain breakage modelling in cohesion-less granular media. *Comput Geotech* 2017;88:199–21.
- [30] Zienkiewicz OC, Chan AHC, Pastor M, Schrefler BA, Shiomi T. Computational geomechanics with special reference to earthquake engineering. New York, USA: John Wiley & Sons Ltd.; 1999.
- [31] Wolf JP. The scaled boundary finite element method. Chichester, UK: Wiley; 2004.
- [32] Chen K, Zou D, Kong X, Chan A, Hu Z. A novel nonlinear solution for the polygon scaled boundary finite element method and its application to geotechnical structures. *Comput Geotech* 2017;82:201–10.
- [33] Zou D, Xu B, Kong X, Liu H, Zhou Y. Numerical simulation of the seismic response of the Zipingpu concrete face rockfill dam during the Wenchuan earthquake based on a generalized plasticity model. *Comput Geotech* 2013;49:111–22.
- [34] Pastor M, Zienkiewicz OC, Chan AHC. Generalized plasticity and the modelling of soil behaviour. *Int J Numer Anal Methods Geomech* 1990;14(3):151–90.
- [35] Liu H, Zou D. Associated generalized plasticity framework for modeling gravelly soils considering particle breakage. *J Eng Mech* 2013;139(5):606–15.
- [36] Ling HI, Yang S. Unified sand model based on the critical state and generalized plasticity. *J Eng Mech* 2006;132(12):1380–91.